



Contents lists available at ScienceDirect

Thermal Science and Engineering Progress

journal homepage: www.sciencedirect.com/journal/thermal-science-and-engineering-progress

An extensive thermo-economic evaluation and optimization of an integrated system empowered by solar-wind-ocean energy converter for electricity generation – Case study: Bandar Abas, Iran

Ehsanolah Assareh^{a,*}, Mohammad Assareh^b, Seyed Mojtaba Alirahmi^a, Saeid Jalilinasrabady^c, Ali Dejdar^a, Mohsen Izadi^d

^a Department of Mechanical Engineering, Dezful Branch, Islamic Azad University, Dezful, Iran

^b Mechanical Engineering Department, Jundi-Shapur University of Technology, Dezful, Iran

^c Department of Earth Resources Engineering, Kyushu University, No. 418 West Building 2, Fukuoka, Japan

^d Department of Mechanical Engineering, Faculty of Engineering, Lorestan University, Iran

ARTICLE INFO

Keywords:

Ocean thermal energy conversion
 OTEC
 Solar energy
 Wind energy
 Integrated system
 NSGA II
 Optimization
 Exergo-economic analysis
 Sensitivity analysis

ABSTRACT

In parallel with efforts to shift human societies' reliance from fossil fuel to renewable resources, in this paper, three green-based energy generation configurations were proposed and examined thermoeconomically. Afterwards, the one with the highest performance was selected for further investigation. The chosen system was empowered by an ocean thermal energy converter (OTEC), a wind turbine, and a solar flat plate panel. The system was modeled by Engineering Equation Solver (EES) software to conduct sensitivity analysis by assessing the impact of changes in objective parameters on the net power output, thermoelectric generator (TEG) power output, exergy efficiency, and cost ratio. In the following steps, EES was coupled with MATLAB through Dynamic Data Exchange (DDE), and a non-dominated sorting genetic algorithm (NSGA-II) was employed for optimizing design parameters including solar panels' area, organic Rankine cycle (ORC) turbine inlet temperature, condenser outlet temperature, ORC pump and turbine efficiency, TEG figure of merit, and evaporator pinch point to reach the highest possible exergy efficiency and the least amount for cost ratio. The system performed with 13.88% exergy efficiency. The exergy destruction analysis showed wind turbine was the most exergy destructor in the system. The configuration is able to generate 448 kW power at its optimal point. Eventually, a case study for Bandar Abbas city, a coastal town in the south of Iran, is carried out to investigate the system's performance concerning the region's potential throughout a year. The results indicate that the system can potentially supply 38 Iranian households with electricity all year-round.

Introduction

The irrefutable truth that incremental global energy demand will definitely render fossil-fuel usage environmentally inviable in the near future has turned eyes toward renewable energies [1,2]. Compared to other renewable energy technologies, solar and wind farms dominate the market due to their impressive price reductions and high accessibility [3,4]. Bearing that in mind, researchers have investigated every conceivable aspect of various green energy production methods to assess the potentials of varying alternative resources. 4E analysis (energy, exergy, economic, environmental analysis) of a biogas-based cogeneration configuration to desalinate water and produce heat, cooling,

power, and hydrogen was conducted by Gargari et al. [5]. Deployment of a solar-wind-based integrated system was tested by Siddiqui and Dincer [6]. Alirahmi and Assareh [7] proposed integrating geothermal and solar energy in a poly-generation system and analyzed it thermoeconomically. More geothermal related works can be found in ref. [8,9]. Two proposed methods for concentrating solar power (CSP) systems, particularly suited for countries of North Africa and the Middle East Studies, by Trucci et al. [10] and Datas et al. [11] are also worthy of being mentioned. Desperately exploring varying green energy exploitation methods, scientists, surprisingly, overlooked or at least paid little attention than it deserved to huge storages for solar energy, which was close at hand, oceanic energy. Ocean thermal energy conversion (OTEC), while being an old idea, has received little attention to the

* Corresponding author.

E-mail address: assareh@iaud.ac.ir (E. Assareh).

<https://doi.org/10.1016/j.tsep.2021.100965>

Received 19 January 2021; Received in revised form 12 May 2021; Accepted 14 May 2021

Available online 21 May 2021

2451-9049/© 2021 Elsevier Ltd. All rights reserved.

Nomenclature		γ	Intercept factor
\dot{E}_X	Exergy Destruction rate, kW	<i>Subscripts and Superscript</i>	
A_p	Collector area, m ²	0	Ambient condition
L	Collector length, m	avg	Average
\dot{Z}	Cost rate \$/h	Cond	Condenser
F1	Collector efficiency factor	D	Destruction
D	Wind turbine diameter, m	Elegant	Efficient Liquid-based Electricity Generation Apparatus
\dot{Q}	Heat rate, kW	Eva	Evaporator
UL	Heat loss coefficient, W/m ² -K	pp	Evaporator pinch point, °C
h_{fi}	Heat transfer coefficient inside the receiver, W/m ² -K	Gen	Generator
M	Mass, kg	HEX	Heat exchanger
\dot{m}	Mass flow rate, kg/s	FR	Heat removal factor
\dot{W}	Net output power, kW	in	Inlet condition
p	Pressure, kPa	IHE	Internal Heat exchanger
RR	Recovery ratio	s	Isentropic
G_b	Solar irradiance, W/m ²	OTEC	Ocean Thermal Energy Conversion
h_x	Specific enthalpy at point x, kJ/kg	OFOH	Open Feedwater Heater
s	Specific entropy, kJ/kg.K	$\tau\alpha$	Optical efficiency
T	Temperature, °C	out	Outlet condition
k	Thermal conductivity, W/m.K	QL	Overall collector heat loss
V	Speed (m/s)	P	Pump
w	Width, m	TEG	Thermo-electric generator
<i>Greek letters</i>		ZTM	TEG figure of merit
α	Absorptivity of the receiver	Tot	Total
ρ	Density, kg/m ³	Tur	Turbine
η	Efficiency, %	Wt	Wind turbine

extent that there are only actual small-scale plants, a 50 kW in Hawaii, after passing almost 140 years from the emergence of the idea. Yet, numerous studies are now being conducted to analyze and optimize them, which illustrates a revival of interest in oceanic energy. In the course of using ocean energy, scientists take advantage of the disparity between water temperature in the deep layers of the ocean and its surface to run a turbine for power generation. The fundamental weakness of OTEC is that the low-temperature difference lessens the net output efficiency. Obviously, the more temperature difference is, the higher the efficiency would be, making it evident that tropical belts for their more temperature difference between surface and deep water are desirable for installing such plants [12–14]. The beauty of OTECs is their stability in terms of temperature difference and availability through night and day simultaneous with a predictability, which enables operators to implement control measures related to seasonal changes in advance [15]. On the flip side, the average efficiency of 3–5% for the Rankine cycles, which are coupled with OTECs, has made the process of power generation pretty costly [16]. To address this problem, one solution is to elevate the relatively low temperature difference between the cool and hot side of the system by heating up the working fluid with another energy resource like solar energy [17]. Interestingly, while several research papers on the investigation of OTEC-primed systems are being published on a yearly basis, compared with studies around other forms of clean energy productions, the recent literature for oceanic-based systems is scarce. In 2019, Khosravi et al. [18] first chose an optimum fluid and then conducted a 3E analysis (energy, exergy, economic analysis) of an ocean thermal energy conversion cycle coupled with a photovoltaic system to produce H₂ and electricity for Islands. The total energy efficiency of around 3.318%, while the exergy performance was between 18% and 19% for the hybrid ocean thermal energy conversion plant. Additionally, their studied configuration was economically cheaper. In 2020, a new renewable system-based configuration supplying ocean thermal energy for district cooling, ammonia, and electricity fabrication was explored by Hassan et al. [19]. Two scenarios

were defined for their recommended system. In the first case, 50% of the generated electricity was stored as ammonia in off-peak hours. The second scenario was designed for peak hours so that the whole power was consumed as electricity. It was reported that for the first scenario, the highest energy and exergy efficiencies were 1.37% and 56.17%, correspondingly. In the second case, while the system's energy performance was as low as 1.83%, the OTEC power plant's exergy efficiency was proved to be 78.02%. Liu et al. [20] recapped previous researches on closed thermodynamic cycles of OTEC. Liu et al. [21] reviewed past research and enhancements on OTEC and open ocean mariculture as they solve a number of urgent problems. Isaac and Dincer [22], to produce clean hydrogen, compared three methods (solar, wind, and OTEC), each of which was integrated with a Cu-Cl-based thermochemical cycle. The calculated energy and exergy performance for wind energy were 33.51% and 32.7%. The thermodynamic efficiencies for solar based methodology were 32.7% for energy and 33.2% for exergy. 5.61% and 13.6% were proved to be energetic and exergetic efficiencies of OTEC based system. In 2019, Bernardoni et al. [23] evaluated and discussed the techno-economic study of an ocean thermal power plant for electricity generation. The efficiency of their proposed system at a temperature difference of 24° C was estimated to be 2.2%. The energy, exergy, and economic performance of an OTEC integrated with a wind turbine was analyzed by Yilmaz [24] for green energy generation in the Mediterranean shores of Turkey to supply a petrol station. For the suggested system, the performance of the whole system and its subsystems were calculated according to the equilibrium equations for mass, energy, entropy, and exergy. Their results revealed that the energetic and exergetic efficiencies of the OTEC plant were 4.49% and 14.84%, concurrently. Wu et al. [25] performed a thermodynamic optimization of the OTEC system with a dual-pressure ORC to make most of the thermal energy. The principal parameters in this system, consisting of sufficient heat transfer plate length, high evaporator temperature, low evaporator temperature, condenser temperature, and volume fraction of a high-pressure turbine, were optimized as target functions. According

to the result, the net power output improved after thermodynamic optimization. Zhou et al. [26] recommended a novel polygeneration system designed to address primary issues in islands. The presented system generated cooling bar, freshwater, and power system. It was demonstrated that multi-effect desalination, generator, and ejectors were the major exergy destructors. The studied system in this research paper performed with exergy efficiency of 29.33%. Khanmohammadi et al. [27] examined a novel solar-assisted OTEC integrated system for hydrogen production. In this study, it was illustrated that usage of TEG along with solar and OTEC system could improve the efficiency by 6.27%. For data prior to 2019 please see Ref. [17,28–32]. Evidently, it is a standard practice for researchers to integrate oceanic energy with other forms of clean resources, especially solar, to enhance efficiency and justify installation of oceanic plants economically. By defining and developing a novel configuration, this study aims to fully exploit the potentials of a coastal city located in tropical belt, where the sun shines directly. In this study, 3 different configurations primed with solar, wind, ocean thermal energy are proposed and compared. After system selection, the chosen one is deeply investigated by Engineering Equation Solver (EES) thermo-economically. The results are first discussed and then compared through a sensitivity analysis. Moreover, an exergy destruction analysis is carried out to give a better understanding of main sources of irreversibilities. EES and MATLAB are linked with a Dynamic Data Exchange (DDE) to run NSGA-II for optimization of design parameters. Lastly, another novelty of the present study is a case study for Bandar Abbas, Iran, which is a heaven for the proposed system due to its extraordinary potentials for wind, solar, and oceanic energy.

System description

The proposed system relies on oceanic energy, solar, and wind power as its energy resources. Three different configurations are assumed and investigated in terms of the first and second laws of thermodynamic by EES to discover the one with the highest functionality. In all three suggested configurations the working fluid is R227ea. Furthermore, a wind turbine backs up the whole system in three planned systems and supplies the pumps. Plan A is illustrated in Fig. 1, for which an organic

Rankine cycle (ORC) is merely coupled with thermal resources for clean electricity production to supply the grid. The ORC perfectly fits the presented systems due to its potentials for full exploitation of low-grade heat. In the Rankine cycle, working fluid absorbs heat from the water, which is pumped out from depths of the ocean and gets heat in solar receivers and then enters the evaporator to warm up the working fluid. The heated working fluid makes its way from evaporator to the turbine to run it. At the end of the cycle, a condenser is designed to cool the working fluid by seawater down to its saturation temperature.

In the planned system for the second scenario, shown in Fig. 2, the system is made up of the same components as plan A; however, instead of a condenser, the system is equipped with an internal heat exchanger (IHE) and an open feedwater heater (OFOH). While IHE in ORC is responsible for heat recovery of low-pressure fluid after the turbine, the OFOH would pre-heat the entering working fluid to the evaporator.

In the third scenario, shown in Fig. 3, the system is made up of the exact same components as plan A; however, instead of a condenser, the system is equipped with a thermoelectric generator (TEG). TEG acts as a condenser along with exploiting the residual heat to for more electricity generation.

System analysis and selection

In this section, the analytical results of the system obtained from EES are presented. According to Fig. 4, which displays the total exergy efficiency of three planned systems, case 3 ranked first with an exergy efficiency of 13.88%.

The net power output of each configuration is illustrated in Fig. 5. Evidently, system three is again placed first by a power production rate of 353.9 kW, followed by case 1 and case 2, respectively.

Regarding Fig. 6, while the least exergy destruction occurs in scenario three, the exergy destruction analysis revealed that scenario one and two destroyed exergy at the rate of 2818.08 and 2820.68 kW, correspondingly. Clearly, the less is the exergy destruction rate, the better is the system.

For economic analysis, an economic model is developed, and the results are shown in Fig. 7. Based on Fig. 7, the three proposed

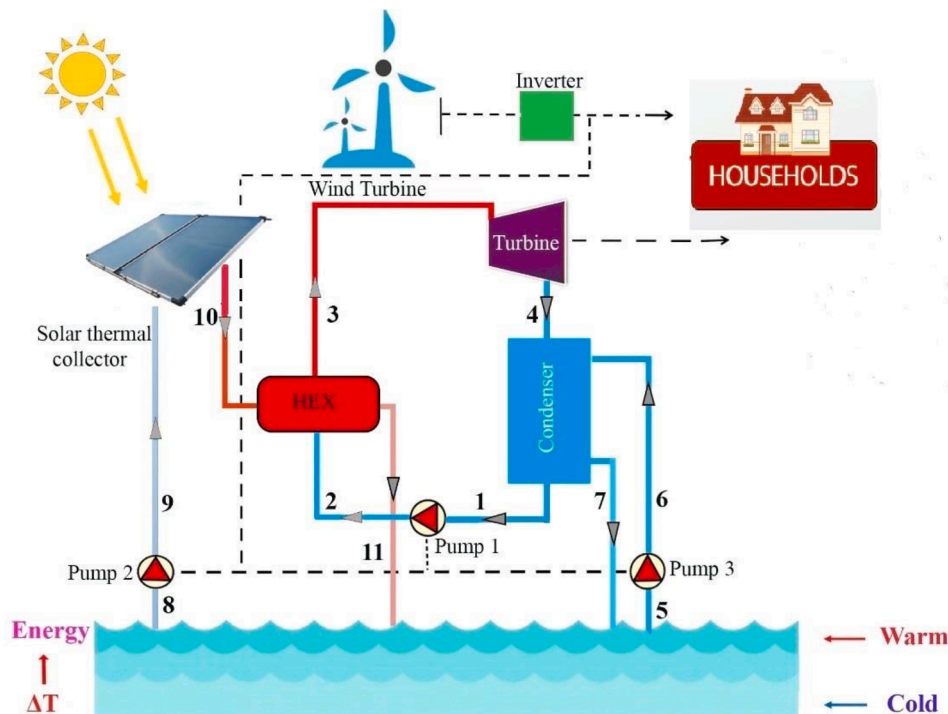


Fig 1. System A: Coupling an ORC with thermal resources (solar and ocean).

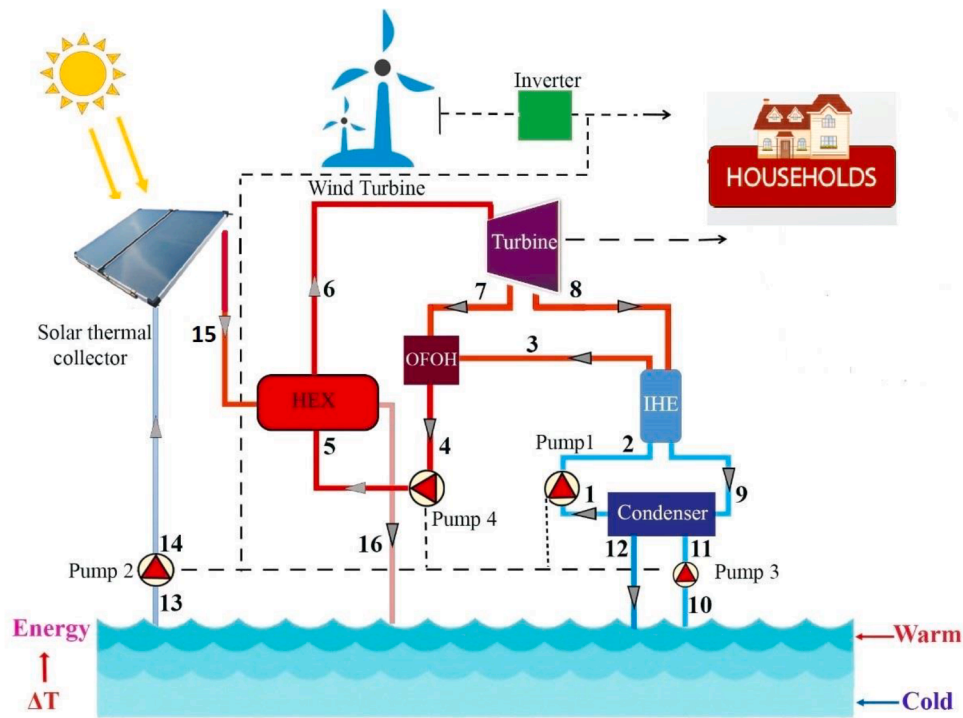


Fig 2. System B: Usage of both a IHE and a OFOH alongside the ORC cycle, which is linked to the thermal resources (solar and ocean).

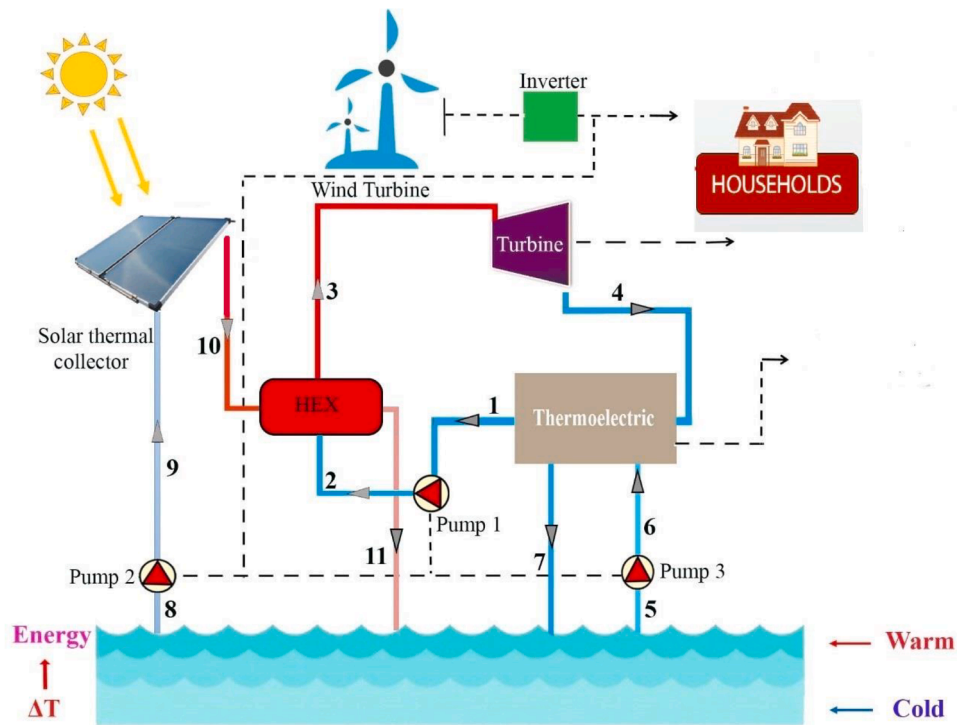


Fig 3. System C: Coupling an ORC cycle with thermal resources (solar and ocean) and usage of a TEG for more electricity production.

configurations' total costs are 2.75×10^6 , 2.82×10^6 , 2.76×10^6 \$, respectively. According to Fig. 7, system A is the best option from the economic aspect, and the worst performance relates to system B.

Overall, system number three is selected for deeper analysis as it outperforms other systems in exergy efficiency, net power output, and exergy destruction rate. Although the total cost in system 3 is 10^4 \$ more than that of system 1, this minor price increase noticeably enhances

generated power of system 3 and its exergy efficiency; therefore, selecting system 3 is justifiable.

Lastly, Table 1 puts the chosen system in the context of literature for providing a brief comparison of recent studies and current work on OTEC. Evidently, higher levels of power generation can be achieved at the cost of lower amounts of exergy efficiency.

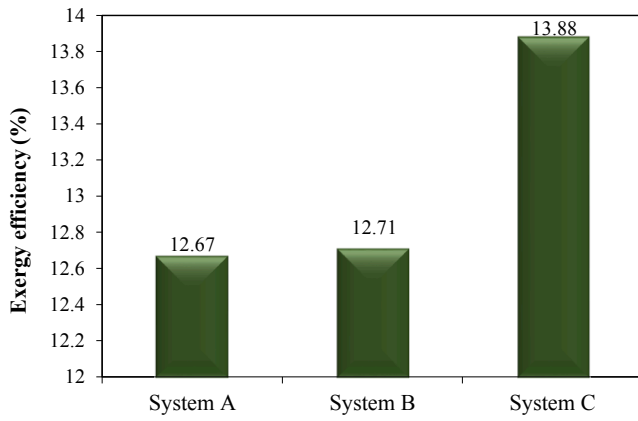


Fig 4. Exergy efficiency of planned systems.

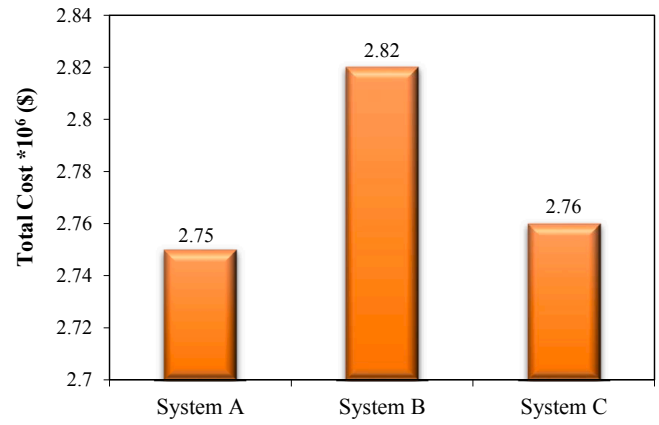


Fig 7. Total cost for various scenarios.

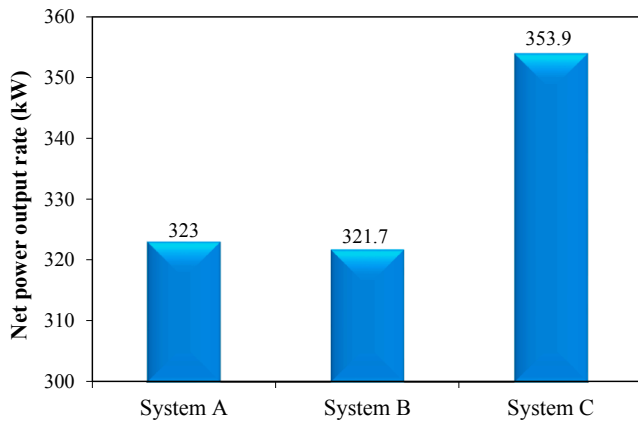


Fig 5. Net power output rate for three planned systems.

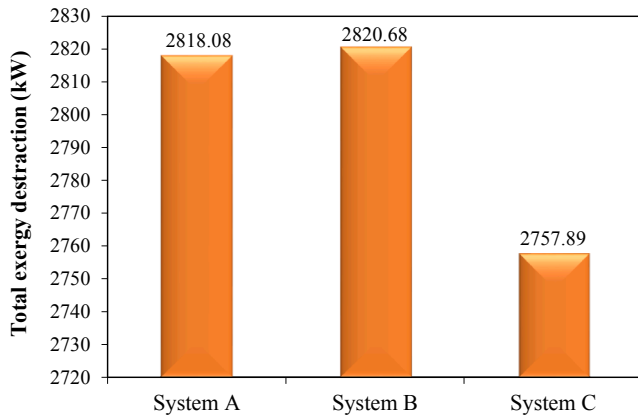


Fig 6. The exergy destruction rate in 3 studied systems.

System modeling

For simplification purposes, each component is treated as a control volume so that the energy and mass balance equations can be applied to govern the primary equations. In the following equations subscript “i” denotes inlet values and subscript “out” denotes outlet values.

$$\sum \dot{m}_{in} = \sum \dot{m}_{out} \tag{1}$$

\dot{m} In equation (1) denotes mass flow rate. The energy balance equation is defined as [33]:

Table 1

Comparison between recent works and presented study.

Row	Ref. number	Author	Exergy efficiency	Net power output (kW)
1	[27]	Khanmohammadi et al.	54.96	110.9
2	[32]	Yilmaz et al.	36.49	–
3	[24]	Yilmaz	23.34	106.4
4	Current study	Assareh et al.	13.88	353.9
5	[31]	Mohd Idrus et al.	4.61	32,593

$$\dot{Q} - \dot{W} = \sum (\dot{m}h)_{out} - \sum (\dot{m}h)_{in} \tag{2}$$

In eq. (2), \dot{Q} and \dot{W} are heat transfer rate and power output rate, respectively. Moreover, all processes are assumed to be in a steady-state condition, and the turbine and pumps are considered adiabatic components [34]. For the studied system (system 3), the initial data for modeling and optimization are shown in Table 2. It is worth mentioning that all temperatures are converted to Kelvin in the EES code.

Table 3 includes the main design and modeling parameters in this study.

Solar flat panel collector

Flat plate panels are deployed as solar receivers for their low cost compared to other solar receivers. The generated heat by the working fluid is obtainable by eq. (1) [28].

$$\dot{Q}_u = \dot{m}C_p(T_{10} - T_9) \tag{3}$$

where \dot{Q}_u is generated heat by solar panels, T_9 is the water inlet temperature at point 9 and T_{10} is the water outlet temperature at point 10.

By employment of the Hottel-Whillier equation, the heat gain of a flat plate is [38]:

$$\dot{Q}_u = A_p F_R [(\tau\alpha)G_b - Q_L] \tag{4}$$

$\tau\alpha$ is the optical efficiency. F_R which is heat removal factor is can be obtained as follows:

$$F_R = \frac{\dot{m}C_p}{U_l A_p} \left[1 - e^{-\left\{ \frac{F_1 U_l A_p}{\dot{m}C_p} \right\}} \right] \tag{5}$$

In Eq. (5), F_1 represents the collector efficiency factor, which is approximately equal to 0.9114, and U_l , the overall collector heat loss. The value for losses can be obtained from the ref [38].

Table 2
Input data for system modeling and optimization [28,35–37].

Parameters	Description	Value
T_0	environment temperature	25 (°C)
A_p	Collector area	10000(m^2)to12000(m^2)
T_8	The temperature of the incoming water from the ocean	30 (°C)
D	Wind turbine diameter	34 (m)
T_{10}	Output temperature of the solar collector	95 (°C)
P_0	Ambient pressure	101.3 (kPa)
P_8	Inlet pressure from the ocean	101.3 (kPa)
P_9	Inlet pressure to the solar collector	150 (kPa)
C_p	Specific heat at constant pressure	4184(J/kg K)
F_1	Collector efficiency factor	0.9114
G_b	Solar irradiance	800($\frac{W}{m^2}$)
T_{sun}	Sun temperature	5770 (K)
U_l	Heat loss coefficient	3.82 (W/ m^2 ·K)
T_3	Heat-exchanger outlet temperature	60 (°C)
T_1	Inlet temperature to pump number 1	15 (°C)
T_5	Inlet temperature to pump number 3	5 (°C)
PP_{Eva}	Pinch Point Evaporator	5 (°C)
PP_{Cond}	Pinch Point Condenser	5 (°C)
η_{pump}	Pump efficiency	0.85 (%)
$\eta_{turbine}$	Turbine efficiency	0.80 (%)
$V_{avg,wind}$	Average wind speed	5.5 (m/s)
η_{wt}	Wind turbine efficiency	0.9
$\eta_{eco-efficiency}$	Eco-efficiency	0.59
ρ_{air}	Air density	1kg/ m^3
$\tau\alpha$	Optical efficiency	0.82

Table 3
Main design and modeling parameters.

Row	Data	Parameter definition
1	PP_{Eva}	Pinch Point Evaporator
2	η_{pump}	Pump efficiency
3	$\eta_{turbine}$	Turbine efficiency
4	$V_{avg,wind}$	Average wind speed
5	T_3	ORC turbine inlet temperature
6	T_1	ORC pump inlet temperature
7	A_p	Collector area
8	ZT_M	TEG figure of merit
9	G_b	Solar irradiance

$$Q_L = U_l(T_{in} - T_0) \quad (6)$$

Thermoelectric generator analysis

TEGs are a type of heat engine in which the electrons play the working fluid's role and convert residual heat from the ORC turbine into electricity. These machines have a lower Power-to-weight ratio than other power generators, and because they have no moving component, they demand little maintenance, which enhances reliability [39]. While the ORC turbine's outlet supplies the warm side of TEG, its cold side is fed with water from the ocean. By installing TEG after the turbine, it plays a condenser role along with exploiting the residual heat of working fluid for more electricity production. The eq. (7) defines the efficiency of TEG [3]:

$$\eta_{TEG} = \eta_{carnot} \times \frac{((\sqrt{1+ZT_M}) - 1)}{(\sqrt{1+ZT_M})} \cdot \frac{(+ (T_L))}{\left(\left(+ \frac{T_L}{T_H} \right) \right)} \quad (7)$$

The following equation is utilized for thermoelectric efficiency [3]:

$$\eta_{TEG} = \frac{\dot{W}_{TEG}}{\dot{Q}_{Elegant}} \quad (8)$$

In eq. (7), ZT_m is the TEG figure of merit, and in eq. (6) Elegant stands for Efficient Liquid-based Electricity Generation Apparatus.

These parameters are defined as below [40,41]:

$$\dot{Q}_{Elegant} = \dot{m}_6(h_7 - h_6) \quad (9)$$

$$\eta_{Carnot} = 1 - \frac{T_L}{T_H} \quad (10)$$

$$T_H = \frac{1}{2}(T_4 + T_1) \quad (11)$$

$$T_L = \frac{1}{2}(T_6 + T_7) \quad (12)$$

Wind turbine

The area of a wind turbine is expressed as [36]:

$$A_{wt} = (D^2) \times (3.14/4) \quad (13)$$

To calculate generated electricity by wind turbine regarding maximum and average wind speed, the following equation can be used [36]:

$$\dot{W}_{wt} = \frac{1}{2} \eta_{wt} \rho_{air} A_{wt} \eta_{ecoefficiency} V_{avg,wind}^3 \times 4/1000 \quad (14)$$

The energy balance equation of each system based on schematic 3 (Fig. 3) is demonstrated in Table 4:

The power output of the whole system based on Table 4 is:

$$\dot{W}_{net} = \dot{W}_{turbine} - \dot{W}_{pump1} - \dot{W}_{pump2} - \dot{W}_{pump3} + \dot{W}_{wt} + \dot{W}_{TEG} \quad (15)$$

The exergy destruction formula related to each component is represented in Table 5:

The amount of exergy destruction of the entire system is computed by the following equation:

$$\dot{E}_{Tot} = \dot{E}_{Collector} + \dot{E}_{Tur} + \dot{E}_{TEG} + \dot{E}_{Pump1} + \dot{E}_{Pump2} + \dot{E}_{Pump3} + \dot{E}_{Eva} + \dot{E}_{Wt} \quad (16)$$

Economic assessment

Due to the importance of the system's economic evaluation, this section represents the needed equations to estimate the purchase and maintenance costs of the 'system's components.

The capital recovery factor (CRF) can be defined as follows [43]:

$$CRF = \frac{i(1+i)^n}{(1+i)^n - 1} \quad (17)$$

The plant's interest rate is denoted by i and is equal to 0.1, and the lifetime period is represented by n and is equivalent to 20 (years). Capital recovery factor (CRF) is obtainable by eq. (18) [43].

$$\dot{Z} = \frac{Z_{total} CRF \phi}{T} \quad (18)$$

Table 4
Energy balance equations of various components based on Fig. 3.

Component	Energy balance equations
pump number 1	
pump number 2	$\dot{W}_{pump2} = \dot{m}_8 \times (h_9 - h_8)$
pump number 3	$\dot{W}_{pump3} = \dot{m}_5 \times (h_6 - h_5)$
Turbine	
ORC cycle	
Evaporator	$\dot{Q}_{Eva} = \dot{m}_{10}(h_{10} - h_{11})$

Table 5
Exergy destruction equations for various components of Fig. 3 [7,42].

Component	Exergy destruction rate equations
Evaporator	$\dot{E}_{Eva} = \dot{E}x_2 + \dot{E}x_{10} - \dot{E}x_{11} - \dot{E}x_3$
pump number 1	$\dot{E}_{pump1} = \dot{E}x_1 + \dot{W}_{pump1} - \dot{E}x_2$
pump number 2	$\dot{E}_{pump2} = \dot{E}x_8 + \dot{W}_{pump2} - \dot{E}x_9$
pump number 3	$\dot{E}_{pump3} = \dot{E}x_5 + \dot{W}_{pump3} - \dot{E}x_6$
Turbine	$\dot{E}_{Tur} = \dot{E}x_3 - \dot{E}x_4 - Ex_{Sun}$
Wind turbine	$\dot{E}_{Wt} = W_{Wt}/\eta$
Thermoelectric	$\dot{E}_{TEG} = \dot{E}x_4 + \dot{E}x_6 - \dot{E}x_7 - \dot{E}x_1 - \dot{W}_{TEG}$
solar collector	$\dot{E}_{Collector} = Ex_{Sun} + \dot{E}x_9 - \dot{E}x_{10}$

Z_{total} , T , and \varnothing denote the total cost, annual working hours, and maintenance factor, correspondingly. \dot{Z} in Eq. (18) denotes the cost rate. And the entire system efficiency (η) is calculated from the following equation:

$$\eta_{ex} = \frac{\dot{W}_{net}}{\dot{E}x_{Sun} + \dot{E}x_{Wind} + \dot{E}x_8} \quad (19)$$

This research paper aims to calculate an optimal point where the costs are minimum and the efficiency is at its maximum possible value.

Necessary equations for cost analysis are illustrated in Table 6 [44,45]:

Results and discussion

Validation

The experimental results from Habibollahzadeh et al. are the yardstick with which the results of this study for TEG are compared to ensure accuracy. Fig. 8 shows the comparison between what the current research has yielded and the case study in ref [41]. According to Fig. 8, a reasonable agreement exists between both works.

Parametric study

Pump

The impact of pump efficiency on varying components of the proposed system is analyzed in this section. According to Fig. 9, the higher pump efficiency is, the higher the system performance would be. This is because the pump efficiency directly relates to the pressure and speed. Although a 20% increase in pump efficiency increases the system’s net power output by around 10 kW, it affects TEG power output only slightly.

Fig. 10 illuminates that higher amounts of pump efficiency enhance exergy efficiency and reduce the cost rate that is highly desirable. Overall, by increasing pump efficiency from 70 to 90 percent, exergy efficiency elevates by roughly 0.4% due to the positive correlation

Table 6
Necessary equations for cost analysis.

Component	Cost balance
Evaporator	$Z_{Eva} = 276 \times (A_{Eva}^{0.88})$
Evaporator area	$A_{Eva} = Q_{Eva} / (u_{Eva} / \Delta T_{ln,Eva})$
pump number 1	
pump number 2	$Z_{pump2} = 3500 \times (\dot{W}_{pump2}^{0.41})$
pump number 3	$Z_{pump3} = 3500 \times (\dot{W}_{pump3}^{0.41})$
Turbine	$Z_{Tur} = 4750 \times (\dot{W}_{tur}^{0.75}) + 60 \times (\dot{W}_{tur}^{0.95})$
Wind turbine	$Z_{Wt} = 5000 \times W_{Wt}$
Thermoelectric	$Z_{TEG} = 1500 \times \dot{W}_{TEG}$
solar collector	$Z_{collector} = 235 \times A_p$

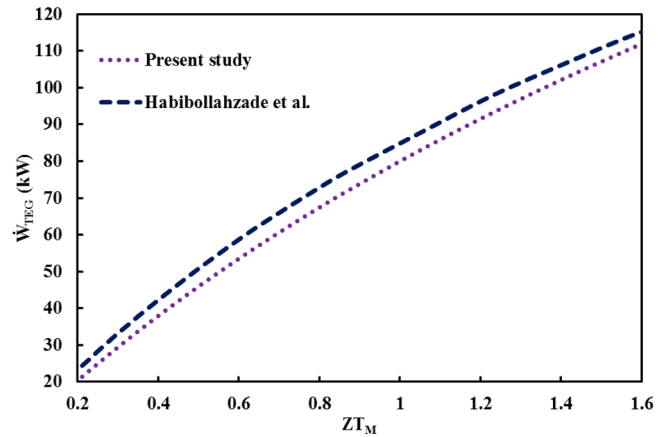


Fig 8. Comparison of the results from this research and work of Habibollahzadeh et al. [41] for TEG.

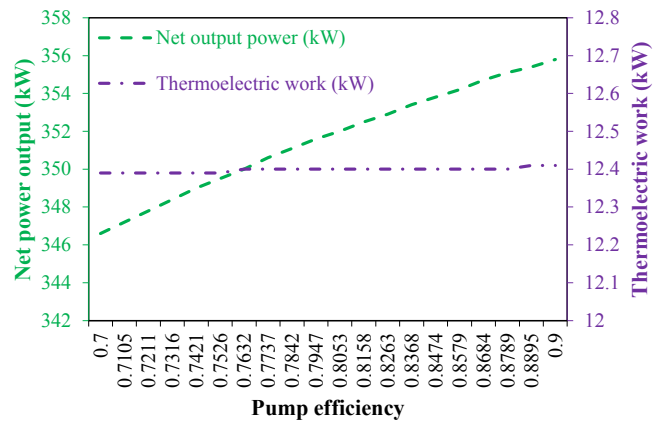


Fig 9. Effect of pump efficiency on net power output and TEG power output.

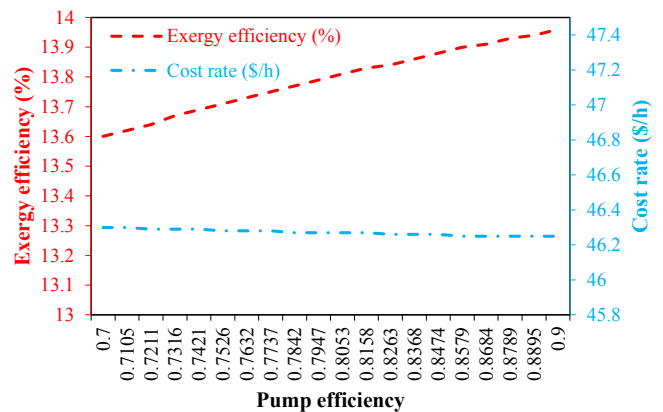


Fig 10. Effect of pump efficiency on exergy efficiency and system cost ratio.

between them, and the cost rate declines by around 0.05%.

The condenser output temperature also leaves a mark on system performance and costs. As illustrated in Fig. 11, a 15 °C growth in temperature from 15 to 30 °C decreases net power output by around 55 kW. Conversely, TEG produced power rises approximately from 12.4 to 20.72 kW with the same increase in the condenser output temperature due to the rise in the TEG inlet fluid’s enthalpy.

While exergy efficiency decreases by enhancing the condenser outlet temperature (Fig. 12), the system cost rate goes up by a negligible

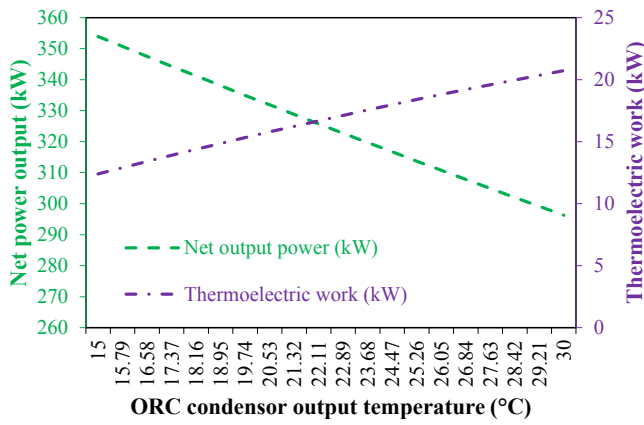


Fig 11. Effect of the ORC pump inlet temperature on net power output and TEG power output.

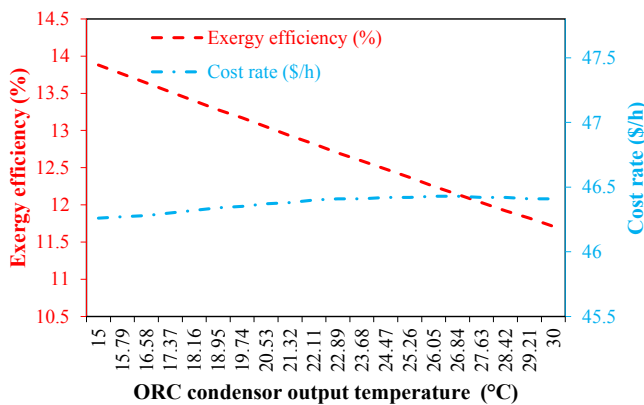


Fig 12. Effect of the ORC pump inlet temperature on exergy efficiency and cost rate.

amount of 0.15 \$/h due to the need for colossal equipment to cool the system. Another reason for this increase can be the need for higher quality material for the ORC pump itself and other equipment as the working temperature increases.

Turbine

The efficiency of the turbine can tremendously affect the performance of the system’s components. Based on Fig. 13, the net power output is significantly under the influence of ORC turbine efficiency. In other words, when turbine efficiency steps up by 20 percent, the net

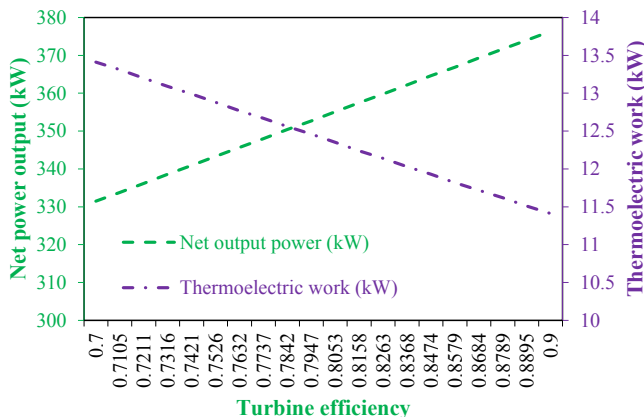


Fig 13. Effect of turbine efficiency on net power output and TEG power output.

power output increases from around 331.5 to 376.4 kW. Oppositely, TEG power output experiences a 21% decline by the same increase in turbine efficiency. Since exergy efficiency and the system’s output are positively related to each other, by enhancing turbine efficiency, exergy efficiency elevates. This statement is confirmed by Fig. 14. However, on the other hand, improving turbine efficiency negatively affects the cost rate by enhancing it. The conflicting nature of the effect of turbine efficiency on exergy efficiency and cost rate heightens the need to find a trade-off point for turbine efficiency. The trade-off point further in the optimization section is discussed in detail.

The ORC turbine inlet temperature also has a significant impact on various components of the system. As shown in Fig. 15, the system’s net power output peaks at 57.8 °C by reaching 355 kW. Both TEG and net power output fall after soaring to a peak. Such behavior is due to the positive correlation between enthalpy and temperature, the increase in temperature results in a rise in enthalpy. Based on Eq. (2), such an increase in enthalpy enhances the power generation. On the other hand, according to the evaporator’s energy balance equation, the evaporator’s temperature increase results in a reduction in flow rate. While at lower temperatures, the first factor has the predominant effect, in temperatures above 57.8 °C it is the second factor that has more influence. Therefore, power generation peaks at 57.8 °C and then declines.

The term related to net power in the numerator of the equation for exergy efficiency is why the graph for both exergy efficiency and net power output behave similarly (Fig. 16). However, at higher temperatures, system costs noticeably decrease.

Evaporator

Fig. 17 represents the influence of the evaporator pinch point on different components. According to this figure, increasing the evaporator pinch point, the system and TEG’s generated power undergoes a significant decrease. The reason engendering this decline in net power output is the reduction in heat transfer from the evaporator to the ORC cycle.

The exergy efficiency reduces from 10.67% to 9.49% because of a severe decline in net power output due to an increase in the evaporator pinch point, as shown in Fig. 18. The cost rate would also decrease with such an increase in the evaporator pinch point.

Wind turbine

The appropriate wind potential of coastal areas justifies the implementation of a wind turbine. The presence of constant fluctuations in wind speed turns the investigation of wind speed changes on various parts of the system of significant importance. Fig. 19 confirms that the net power output considerably depends on wind speed as it increases by almost 370% when the average speed sees a 4 m/s (17 km/h) rise.

Fig. 20 illustrates that at high wind speeds, around 10 m/s (36 km/h), the exergy efficiency of 50% is achievable; however, the higher wind

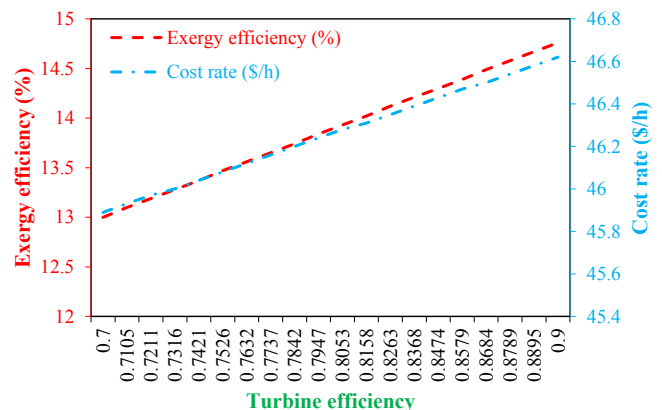


Fig 14. Effect of turbine efficiency on exergy efficiency and cost rate.

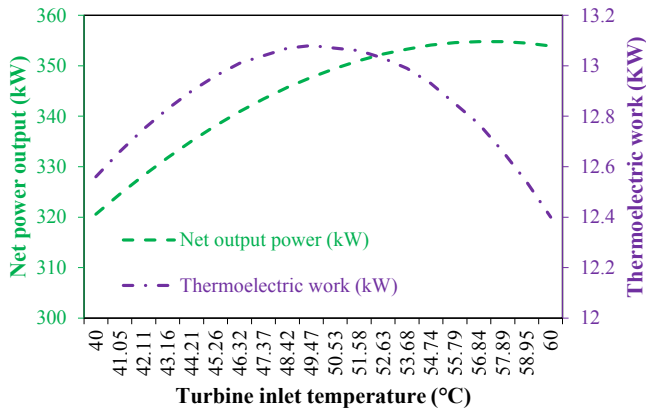


Fig 15. Effect turbine inlet temperature on net power output and TEG power output.

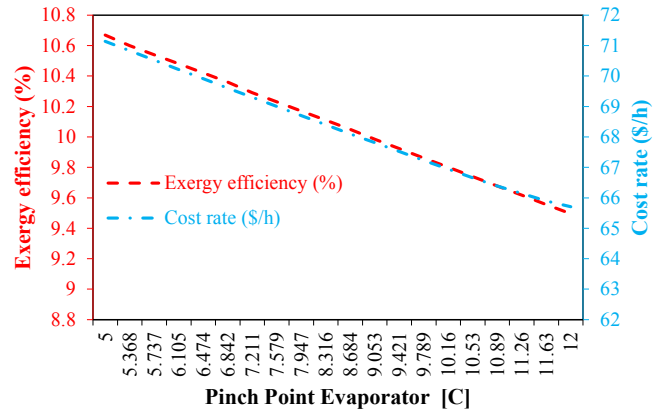


Fig 18. Effect of evaporator pinch point on exergy efficiency and cost rate.

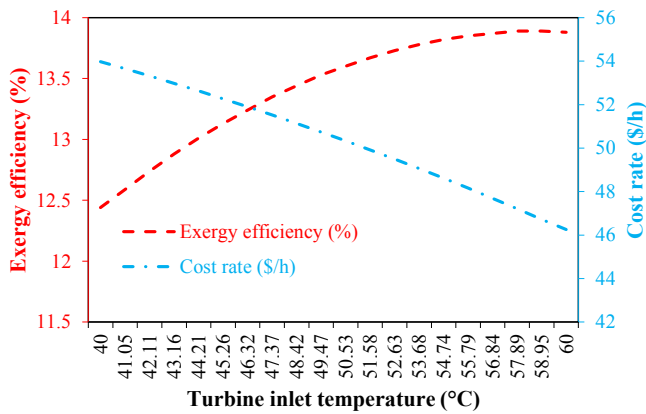


Fig 16. Effect of turbine inlet temperature on exergy efficiency and cost rate.

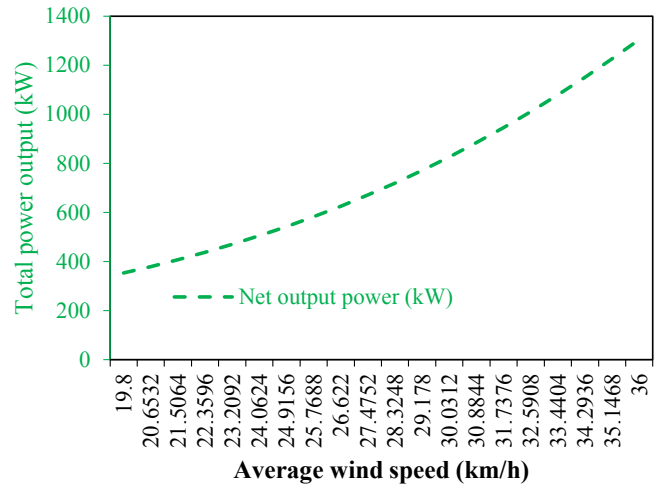


Fig 19. Effect of wind speed on the net power output of the system and TEG output power.

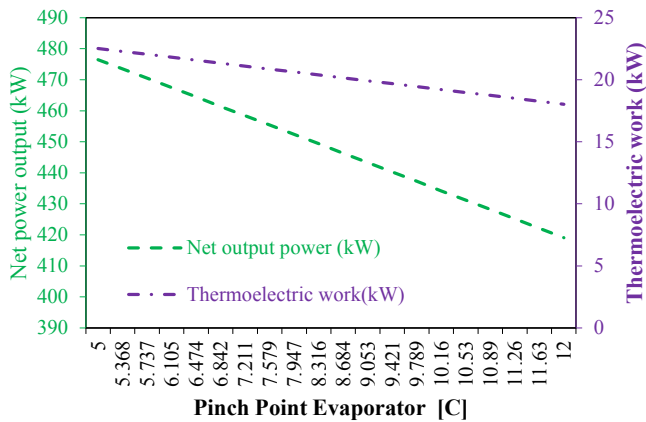


Fig 17. Effect of evaporator pinch point on net power output and TEG power output.

speeds result in more expenses. This increase in the system costs roots in 2 issues: the higher need for more powerful turbines and more maintenance in regions with high wind potentials.

Solar irradiance

The very fact that solar irradiance is the most determining factor in system performance makes studying the effects of its changes crucially important. To elaborate on it more, by enhancing solar irradiance, the turbine's entering flow rate increases. Consequently, the net power

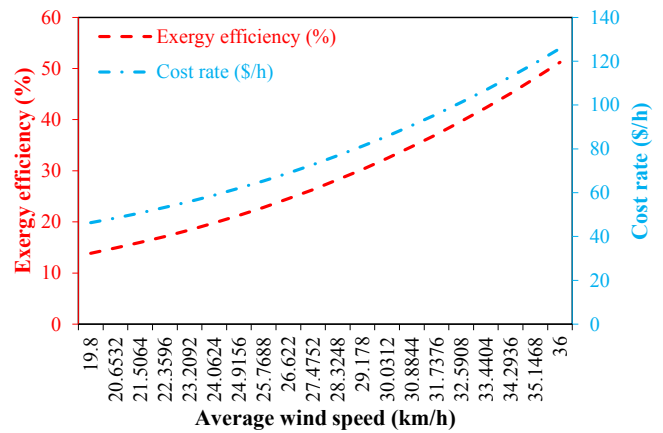


Fig 20. Effect of wind speed on exergy efficiency and cost rate.

output of subsystems and the whole system will go up. According to Fig. 21, an 80% increase in solar irradiance can enhance the net power output and TEG power output by more than 55% and 160%.

According to Fig. 22, exergy efficiency negatively correlates with solar irradiance and decreases at higher solar irradiance. According to Eq. (19), although both its numerator and denominator go up when the solar irradiance rises, the increase in the denominator is steeper. The

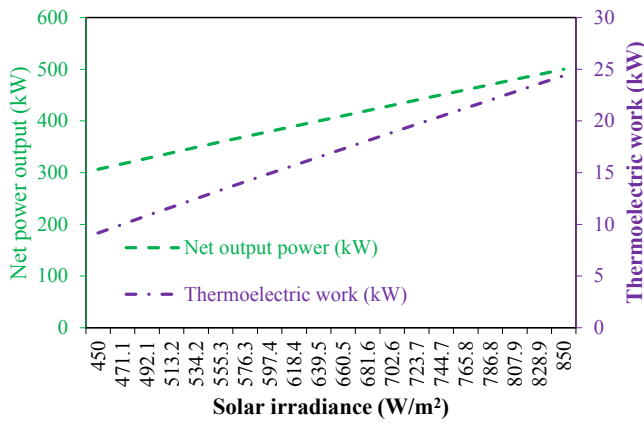


Fig 21. Effect of solar irradiance on net power output and TEG power output.

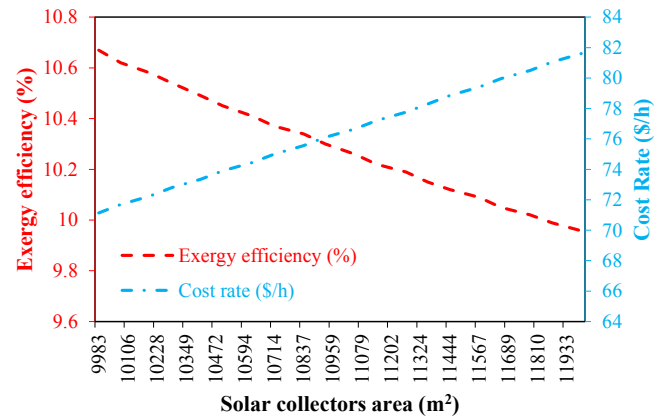


Fig 24. Effect of collector area on exergy efficiency and cost rate.

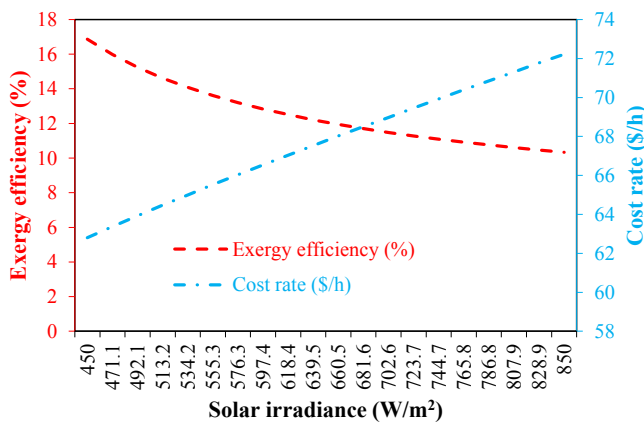


Fig 22. Effect of solar irradiance on exergy efficiency and cost rate.

higher rise in denominator negatively affects exergy efficiency. However, on the flip side, the costs increase by elevating solar irradiance as the net power output is greater at high levels of solar irradiance.

Collector area

Fig. 23 and Fig. 24 demonstrate that all studied criteria experience an increase except exergy efficiency, which falls down by enhancing collector area. In other words, the more collector area is, the more energy absorption would take place. Therefore, an increase in solar energy absorption elevates the net power output from TEG and the whole system. The rise in costs results from an increase in maintenance and

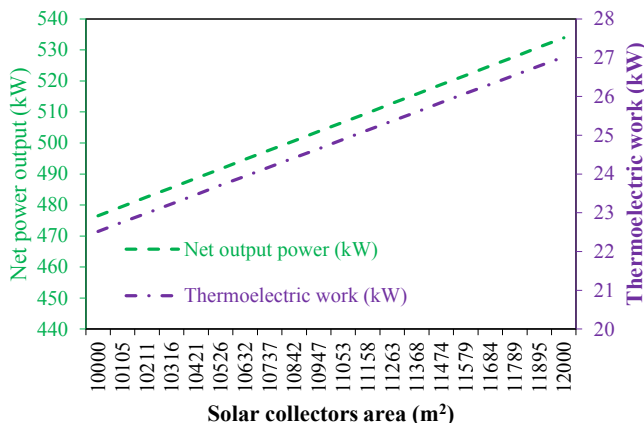


Fig 23. Effect of collector area on net and TEG power output.

installation costs when the collector area is greater.

TEG figure of merit

The figure of merit determines the usefulness of material in TEG. Its amount hinges on the material’s electrical and thermal conductivity and Seebeck coefficient, which change with temperature. Based on Fig. 25, by increasing the TEG figure of merit, both net and TEG power output increase by almost 28 kW. This positive correlation proves the existence of a relationship between a substance’s capability to produce electricity and the figure of merit.

Fig. 26 demonstrates that exergy efficiency behaves in similar fashion as net power output because they are positively related. On the other hand, the augmentation in net power output and exergy efficiency causes the system costs to step up because higher levels of power production are achieved at the expense of installing more expensive equipment. Moreover, higher power production causes more maintenance costs.

Sensitivity analysis

To determine how varying values for different variants affect performance parameters, a sensitivity analysis is conducted. According to Table 7, nothing is more influential than average wind speed as a 5 m/s change in its speed can affect costs and output more than 150%. ORC condenser output temperature is ranked next. The positive point about the ORC condenser output temperature is that it can significantly improve system outputs without making a notable rise in costs if it is accurately designed. Among the studied parameters, ORC pump efficiency leaves the slightest mark on system performance and costs.

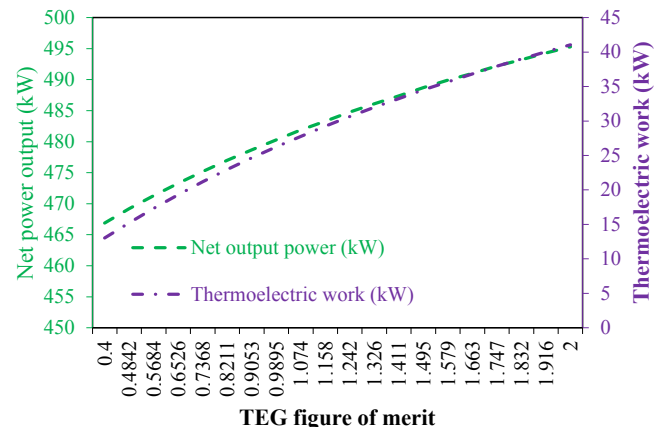


Fig 25. Effect of TEG figure of merit on net and TEG power output.

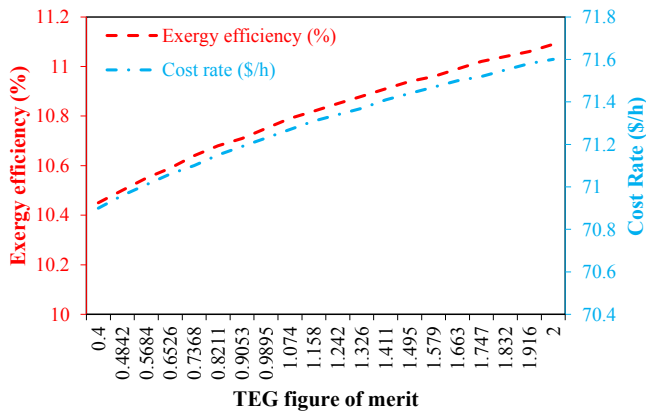


Fig. 26. Effect of TEG figure of merit on exergy efficiency and cost rate.

Exergy destruction analysis

This section revolves around exergy destruction analysis. This criterion shows the amount of lost exergy in the system.

Fig. 27 shows the extent to which pump efficiency affects the system’s exergy destruction rate. These components include pumps (numbers 1, 2, and 3), evaporator, and ORC turbine. The highest rate of exergy destruction relates to the pump (number 3), which decreases with increasing the pump’s efficiency. Pump number 1 is ranked third for exergy destruction. The lowest amount of exergy destruction belongs to pump 2, which is between 10 and 0. Overall, as the efficiency increase, exergy destruction in all 3 pumps reduces. This reduction is because of improvement in pumps’ abilities to turn more electricity into net output work. Yet, this destruction is lower in pump 2 since its work is lower than other pumps. The exergy destruction for the evaporator and ORC turbine is 100 and 45 kJ, respectively. According to the chart, the increase in pump efficiency results in a severe decrease in exergy destruction rate.

Fig. 28 indicates how the evaporator pinch point affects the exergy destruction of the ‘configuration’s components. In the diagram, the ORC turbine exergy destruction is higher than the other components. We found that the rate of exergy destruction reduces by the growth of evaporator temperature. This reduction is because when the evaporator temperature increases, the enthalpy of input fluid to the ORC turbine soars, and the mass flow of R227ea declines. Therefore, the produced power, the exergy efficiency, and the ORC’s cost rate have an optimal point relative to the evaporator temperature.

Fig. 29 proves that the exergy destruction rate in pumps number 1, number 3, and in the evaporator is highly dependent on ORC turbine inlet temperature as they experience the most changes in various turbine inlet temperatures. The rise in turbine inlet temperature enhances the pressure. This enhancement means that the pump has to increase the ‘fluid’s pressure more. Therefore, the increase in exergy destruction is reasonable. Since exergy destruction in pump 2 is irrespective of turbine inlet temperature, the temperature changes do not affect pump 2. Contrary to pump 1, the elevation of turbine inlet temperature reduces the exergy destruction in pump 3. This increase in temperature results in a reduction in fluid flow, so the need for cooling reduces. The effect of turbine inlet temperature on exergy destruction in the evaporator is similar to pump 3. By increasing the turbine inlet temperature, the temperature difference of the two sides of the evaporator decreases, and so does the exergy destruction. Evidently, the exergy destruction in pump 2 is irrespective of turbine inlet temperature. While exergy destruction in pump 1 increases by enhancing turbine inlet temperature, concerning the severe decrease in exergy destruction of the evaporator and pump 3 at higher turbine inlet temperatures, we concluded that the exergy destruction falls by elevating turbine inlet temperature.

Table 7 Sensitivity analysis results.

Row	Parameter	Output			
		Cost rate (\$/h)	Exergy efficiency (kJ)	TEG power output (kW)	net power output (kW)
1	Pump efficiency	Max: 46.3 Min: 46.25 Percent change: 0.1	Max: 13.96 Min: 13.6 Percent change: 1.62	Max: 12.41 Min: 12.39 Percent change: 0.2	Max: 355.8 Min: 346.6 Percent change: 1.62
2	Turbine efficiency	Max: 46.62 Min: 45.89 Percent change: 1.61	Max: 14.76 Min: 13 Percent change: 13.71	Max: 13.41 Min: 11.41 Percent change: 20.49	Max: 376.4 Min: 331.5 Percent change: 13
3	Turbine inlet temperature	Max: 53.98 Min: 46.26 Percent change: 16.39	Max: 13.88 Min: 12.44 Percent change: 9.06	Max: 12.56 Min: 12.4 Percent change: 11.71	Max: 353.9 Min: 320.6 Percent change: 9.53
4	Condenser outlet temperature	Max: 46.41 Min: 46.26 Percent change: 0.2	Max: 13.88 Min: 11.71 Percent change: 19.99	Max: 20.72 Min: 12.4 Percent change: 55.92	Max: 353.9 Min: 296.3 Percent change: 19.98
5	Evaporator pinch point	Max: 71.14 Min: 65.71 Percent change: 16.39	Max: 10.67 Min: 9.495 Percent change: 9.06	Max: 22.52 Min: 18.03 Percent change: 11.71	Max: 476.5 Min: 419.1 Percent change: 9.05
6	Average wind speed	Max: 125.8 Min: 46.26 Percent change: 173.8	Max: 51.2 Min: 13.88 Percent change: 260.9	Max: 12.4 Min: 12.4 Percent change: 0	Max: 1305 Min: 353.9 Percent change: 260.94
7	TEG figure of merit	Max: 71.6 Min: 70.9 Percent change: 0.18	Max: 11.09 Min: 10.45 Percent change: 1.33	Max: 41.04 Min: 13.01 Percent change: 69.41	Max: 495.3 Min: 466.9 Percent change: 1.33
8	Solar irradiance	Max: 72.22 Min: 62.8 Percent change: 47.65	Max: 16.87 Min: 10.34 Percent change: 13.21	Max: 24.38 Min: 9.155 Percent change: 146.68	Max: 500.2 Min: 306.4 Percent change: 63.43
9	Collector’s area	Max: 81.6 Min: 71.14 Percent change: 12.83	Max: 10.67 Min: 9.958 Percent change: 1.88	Max: 27.02 Min: 22.52 Percent change: 16.12	Max: 533.9 Min: 476.5 Percent change: 16.2

Optimization

In this research, the NSGA-II algorithm is utilized for optimizing the design parameters and objective functions. The design variables and their allowable values are represented in Table 8. For multi-objective optimization, the EES and MATLAB software is coupled via a code called Dynamic Data Exchange (DDE) [46]. There is not one specific optimum value in such problems; instead, there are a set of optimum values that are represented as a Pareto boundary. In other words, the most optimum values of design variables for which our objective functions, exergy efficiency, and cost ratio are fulfilled to the best possible extent are represented on the Pareto boundary Fig. 30. While all

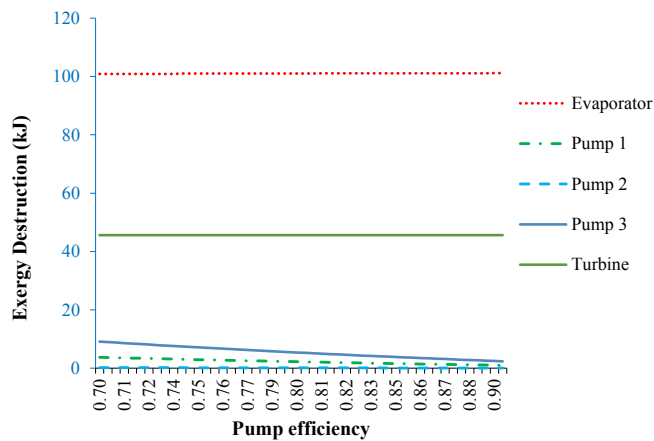


Fig 27. The effect of pump efficiency on the amount of exergy destruction of the system’s components.

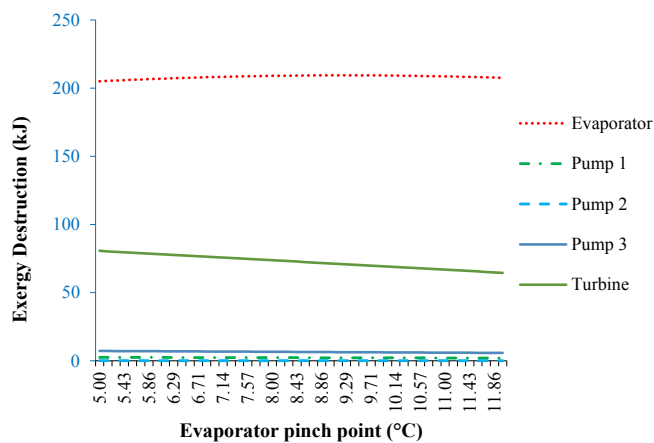


Fig 28. Effect of evaporator pinch point on exergy destruction of different components.

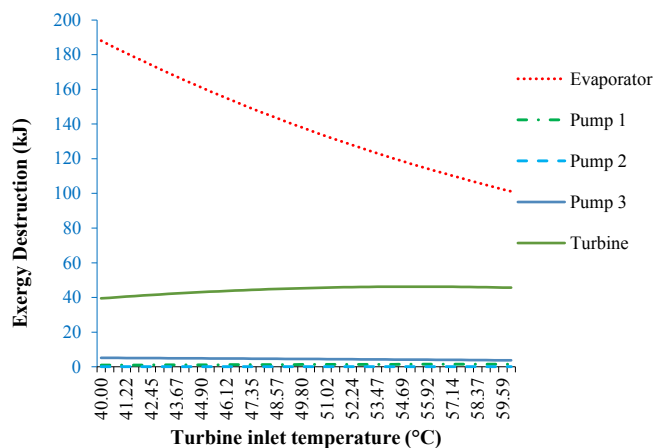


Fig 29. Effect of ORC turbine inlet temperature on exergy destruction of various components.

illustrated points in Fig. 30 are optimum, to pinpoint the Pareto boundary’s best point, a simple geometric method is applied, and its results are shown in Table 9. Based on the Pareto boundary, the most desirable exergy efficiency can be achieved when the cost ratio is at its worst value and vice versa. In other words, the most optimal point for each of the objective functions achieves only at the expense of the worst condition

Table 8
The design variables and the range of changes.

Parameter	Lower bound	Upper bound
A_p (m ²)	8000	12,000
T_1 (°C)	15	30
T_3 (°C)	40	60
PP_{Eva} (°C)	2.5	6.5
η_{pump}	0.7	0.9
$\eta_{Turbine}$	0.7	0.9
ZT_m	0.5	1.5

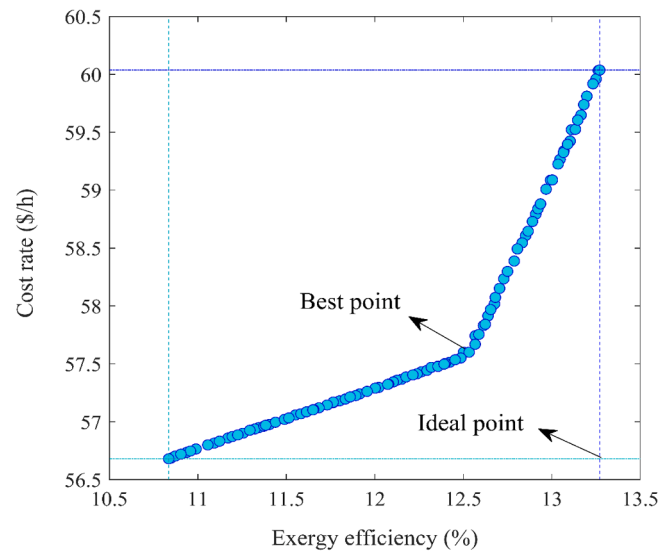


Fig 30. Pareto boundary of the optimal points of the proposed system.

Table 9
Optimal objective functions.

Objective function	Value
Exergy efficiency (%)	12.53
Cost rate (\$/h)	57.6

for the other one. According to the Pareto boundary, the ideal point is unachievable due to thermodynamic irreversibilities. Through a geometric method, the closest point to the ideal point is chosen as the most optimal point (Best point).

Further information on the optimum point and optimization parameters is represented in Tables 9 and 10.

According to the optimization results, the system is capable of producing 448 kW power at optimal conditions. ORC turbine accounts for 277.6 kW of the whole generated electricity, and the rest is produced by wind turbine and TEG by an amount of 190 and 22.7 kW, respectively. Pumps consume 42.3 kW of the produced energy.

Table 10
Optimization parameters.

Optimization parameters	Value
A_p	8060 m ²
T_1	15.21 °C
T_3	59.98 °C
PP_{EVA}	6.46 °C
η_{pump}	0.9
$\eta_{Turbine}$	0.9
ZT_m	1.4

a year on net output work.

Case study (Bandar Abbas City)

Bandar Abbas is a coastal city located in the southern part of Iran. The city receives a suitable amount of sunlight and wind all year round, so the city is a perfect spot for implementing our proposed system. Due to the high level of solar irradiance in this area, the surface water receives an ample amount of solar energy and stores it as heat. This process warms up the water and enhances the temperature difference between the surface and the depth of water. Therefore, as discussed in previous sections, the more is the temperature difference, the more would be the efficiency and generated power in the proposed system. Moreover, since wind speed is the most influential factor according to sensitivity analysis, the abundance of wind energy in Bandar Abbas justifies implementing the studied system. Fig. 31 shows the location of the city on the map.

The variances in the average wind speed, temperature, and solar irradiance during a year for Bandar Abbas are shown in Figs. 32, 33, and 34, correspondingly. All the data are extracted from Meteonorm software.

The following charts examine the variances in wind speed, ambient temperature, and solar irradiance during a year on an hourly basis, on the system's net output, total exergy efficiency, and system costs. Fig. 35 shows the impact of wind speed changes during a year on net output work. According to this figure, the month's maximum amount of work is 223391.1 kWh for July and August.

Fig. 36 shows the results for the effect of year-round wind speed changes on exergy efficiency. Regarding this figure's result, the highest amount of net output work is for July, which has a value of 11.77%.

Fig. 37 shows the results for the influence of solar irradiance changes throughout a year on exergy efficiency. According to this figure, the highest amount of net output work is for December. Since the solar irradiance, less than 350 W/m^2 , has a little negligible effect on power production, more than 350 W/m^2 are taken into account.

Fig. 38 shows the results for the impact of solar irradiance changes throughout a year on net output work. Based on this figure, the maximum amount of net output work is 105254.252 kWh in April.

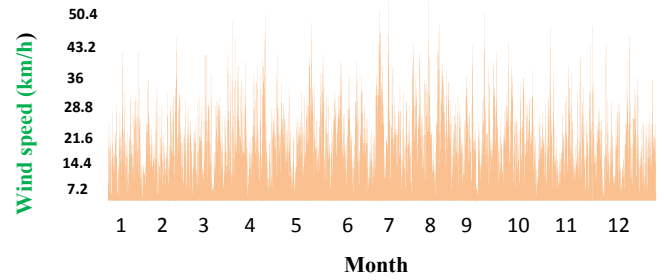


Fig 32. Bandar Abbas average wind speed during a year.

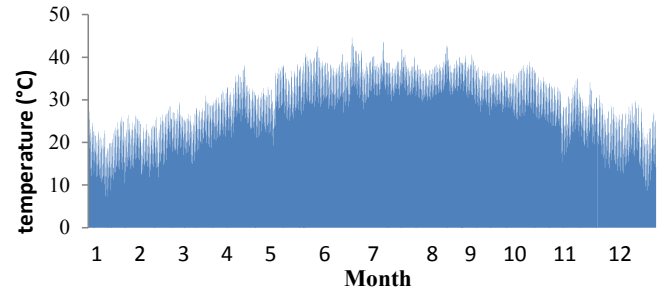


Fig 33. Temperature changes of Bandar Abbas during a year.

Fig. 38 is used to approximate the amount of net output work by the proposed configuration in the studied region for a year. To simplify the calculation, in addition to considering a constant temperature difference throughout a year between the cold and hot surface of water, an average wind speed throughout a year for Bandar Abbas, according to data, is assumed. Due to the considerable changes in solar irradiance, its variance based on data is completely taken into account. According to Fig. 38, the system can generate 1131966.058 kWh in a year. Based on a



Fig 31. Location of Bandar Abbas on the map.

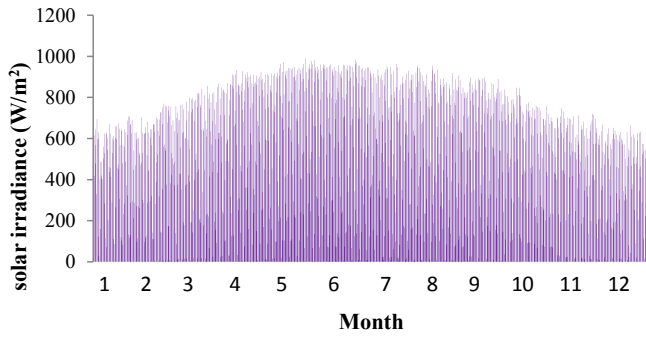


Fig 34. Average solar irradiance in Bandar Abbas during a year.

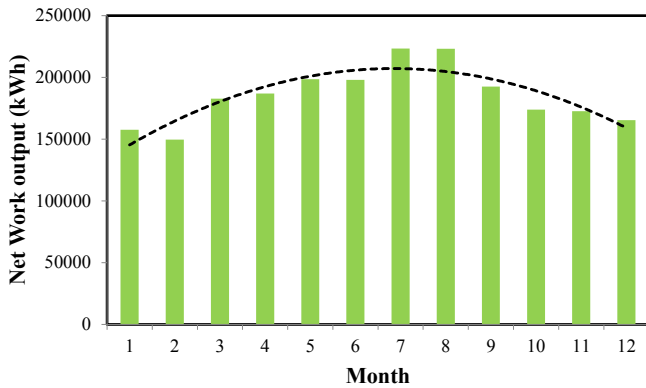


Fig 35. Effect of wind speed changes throughout a year on net output work.

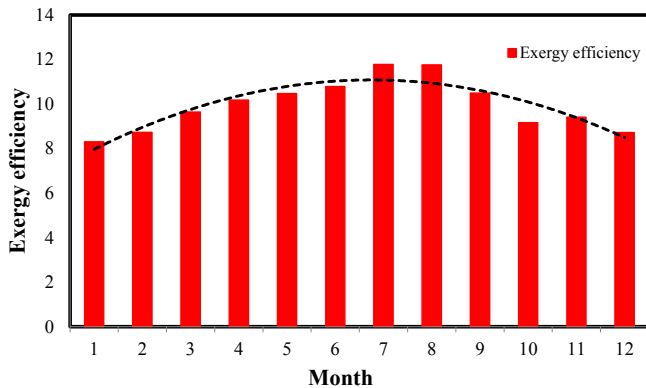


Fig 36. Effect of year-round wind speed changes throughout a year on exergy efficiency.

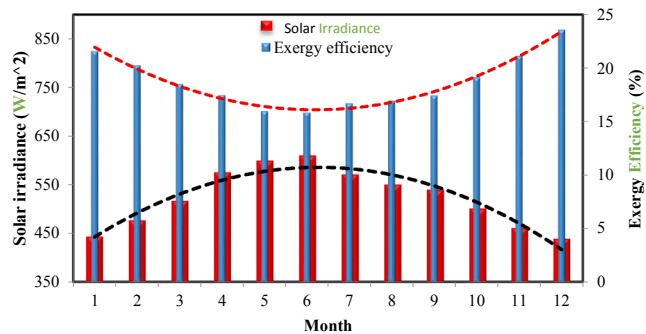


Fig 37. Effect of year-round solar irradiance changes throughout a year on exergy efficiency.

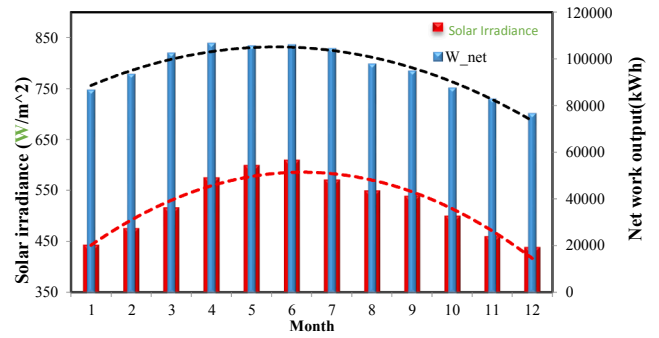


Fig 38. Effects of solar irradiance changes throughout.

2010 report from the ministry of energy of Iran, the average electricity consumption of an Iranian household is around 29,172 kWh; therefore, the system can meet the need of 38 households throughout a year.

Conclusions

The ever-increasing demand for electricity and scarce fossil-fuel resources have pushed researchers to think of alternative energy resources as a solution. In this work, 3 energy systems based on solar, wind, and OTEC were analyzed. The systems were designed for an area with appropriate ocean thermal energy, wind energy, and solar energy, mainly located in the tropical belt. After evaluation, ultimately, the one with the best performance was selected for further investigation. The chosen system consisted of a combination of subsystems, including a flat panel solar collector, OTEC system, wind turbine, ORC, and a thermo-electric. The proposed system was designed and evaluated based on the average yearly electricity consumption required by an Iranian household. In this Study, the R227ea refrigerant was applied as an organic fluid in the ORC and water for the OTEC system. EES software was utilized as an engineering tool to model the system and obtain thermodynamic results. After sensitivity analysis, the most significant and influential parameters were proved to be wind speed, ORC pump inlet temperature, solar irradiance, and collector area. Eventually, the system was optimized via NSGA-II.

To summarize the results

- While replacement of compressor with other equipment could improve the system’s thermodynamic performance, the combination of TEG and recuperator was not as effective as a single TEG was.
- Average wind speed and ORC pump inlet temperature were the most impactful parameters on the system performance.
- Elevating wind speed improves total work and exergy efficiency at the expense of a significant soar in system costs.
- The wind turbine and the connected pump to the TEG module were responsible for the most of destructed exergy
- Working at optimum condition, the system performed at exergy efficiency and cost rate of 12.53%, 57.6 \$/h, correspondingly.
- The associated net power output at the optimal point was 448 kW, and most of this amount was generated by the ORC turbine.
- The system can meet the electricity demand of 38 Iranian households during a year.

CRedit authorship contribution statement

Ehsanolah Assareh: Supervision, Methodology, Software, Validation. **Mohammad Assareh:** Writing - original draft, Methodology, Software. **Seyed Mojtaba Alirahmi:** Visualization, Investigation, Methodology, Software, Validation. **Saeid Jalilinasrabad:** Writing - review & editing, Supervision. **Ali Dejdard:** Writing - original draft. **Mohsen Izadi:** Supervision.

Declaration of Competing Interest

The authors declare that they have no known competing financial interests or personal relationships that could have appeared to influence the work reported in this paper.

References

- [1] S.M. Alirahmi, S. Bashiri Mousavi, A.R. Razmi, P. Ahmadi, A comprehensive techno-economic analysis and multi-criteria optimization of a compressed air energy storage (CAES) hybridized with solar and desalination units, *Energy Convers. Manag.* 236 (2021) 114053, <https://doi.org/10.1016/j.enconman.2021.114053>.
- [2] M.H. Nabat, M. Zeynalian, A.R. Razmi, A. Arabkoosar, M. Soltani, Energy, exergy, and economic analyses of an innovative energy storage system; liquid air energy storage (LAES) combined with high-temperature thermal energy storage (HTES), *Energy Convers. Manag.* 226 (2020) 113486, <https://doi.org/10.1016/j.enconman.2020.113486>.
- [3] S.M. Alirahmi, A.R. Razmi, A. Arabkoosar, Comprehensive assessment and multi-objective optimization of a green concept based on a combination of hydrogen and compressed air energy storage (CAES) systems, *Renew. Sustain. Energy Rev.* 142 (2021) 110850, <https://doi.org/10.1016/j.rser.2021.110850>.
- [4] A.R. Razmi, M. Soltani, A. Ardehali, K. Gharali, M.B. Dusseault, J. Nathwani, Design, thermodynamic, and wind assessments of a compressed air energy storage (CAES) integrated with two adjacent wind farms: A case study at Abhar and Kahak sites, *Iran, Energy*. 221 (2021) 119902, <https://doi.org/10.1016/j.energy.2021.119902>.
- [5] S.G. Gargari, M. Rahimi, H. Ghaebi, Energy, exergy, economic and environmental analysis and optimization of a novel biogas-based multigeneration system based on Gas Turbine-Modular Helium Reactor cycle, *Energy Convers. Manag.* 185 (2019) 816–835, <https://doi.org/10.1016/j.enconman.2019.02.029>.
- [6] O. Siddiqui, I. Dincer, Design and analysis of a novel solar-wind based integrated energy system utilizing ammonia for energy storage, *Energy Convers. Manag.* 195 (2019) 866–884, <https://doi.org/10.1016/j.enconman.2019.05.001>.
- [7] S.M. Alirahmi, E. Assareh, Energy, exergy, and exergoeconomics (3E) analysis and multi-objective optimization of a multi-generation energy system for day and night time power generation - Case study: Dezful city, *Int. J. Hydrogen Energy*. 45 (56) (2020) 31555–31573, <https://doi.org/10.1016/j.ijhydene.2020.08.160>.
- [8] S. Jalilinasrabad, R. Itoi, H. Gotoh, H. Kamenosono, Energy and Exergy Analysis of Takigami Geothermal Power Plant, Oita, Japan, *GRC Transactions*. 34(2010), Request PDF, (n.d.). https://www.researchgate.net/publication/215536082_Energy_and_Exergy_Analysis_of_Takigami_Geothermal_Power_Plant_Oita_Japan (accessed May 12, 2021).
- [9] S. Jalilinasrabad, R. Itoi, P. Valdimarsson, G. Saevarsdottir, H. Fujii, Flash cycle optimization of Sabalan geothermal power plant employing exergy concept, *Geothermics*. 43 (2012) 75–82, <https://doi.org/10.1016/j.geothermics.2012.02.003>.
- [10] D.M. Trucchi, A. Bellucci, M. Girolami, P. Calvani, E. Cappelli, S. Orlando, R. Polini, L. Silvestroni, D. Sciti, A. Kribus, Solar Thermionic-Thermoelectric Generator (ST² G): Concept, Materials Engineering, and Prototype Demonstration, *Adv. Energy Mater.* 8 (32) (2018) 1802310, <https://doi.org/10.1002/aenm.v8.3210.1002/aenm.201802310>.
- [11] A. Datas, A.B. Cristobal, C. Del Cañizo, E. Antolín, M. Beaughon, N. Nikolopoulos, A. Nikolopoulos, M. Zeneli, N. Sobczak, W. Polkowski, M. Tangstad, J. Safarian, D. M. Trucchi, A. Bellucci, M. Girolami, R. Marx, D. Bestenlehner, S. Lang, A. Vitulano, G. Sabbatella, A. Martí, AMADEUS: Next generation materials and solid state devices for ultra high temperature energy storage and conversion, in: *AIP Conf. Proc.*, American Institute of Physics Inc., 2018: p. 170004. <https://doi.org/10.1063/1.5067168>.
- [12] K. Rajagopalan, G.C. Nihous, Estimates of global Ocean Thermal Energy Conversion (OTEC) resources using an ocean general circulation model, *Renew. Energy*. 50 (2013) 532–540, <https://doi.org/10.1016/j.renene.2012.07.014>.
- [13] M. Faizal, M.R. Ahmed, Experimental studies on a closed cycle demonstration OTEC plant working on small temperature difference, *Renew. Energy*. 51 (2013) 234–240, <https://doi.org/10.1016/j.renene.2012.09.041>.
- [14] P. Bombarda, C. Invernizzi, M. Gaia, Performance analysis of OTEC plants with multilevel organic rankine cycle and solar hybridization, *J. Eng. Gas Turbines Power*. 135 (2013), <https://doi.org/10.1115/1.4007729>.
- [15] J.-I. Yoon, C.-H. Son, S.-M. Baek, B.H. Ye, H.-J. Kim, H.-S. Lee, Performance characteristics of a high-efficiency R717 OTEC power cycle, *Appl. Therm. Eng.* 72 (2) (2014) 304–308, <https://doi.org/10.1016/j.applthermaleng.2014.05.103>.
- [16] N. Yamada, A. Hoshi, Y. Ikegami, Performance simulation of solar-assisted ocean thermal energy conversion plant, *Renew. Energy*. 34 (7) (2009) 1752–1758, <https://doi.org/10.1016/j.renene.2008.12.028>.
- [17] H. Yuan, P. Zhou, N. Mei, Performance analysis of a solar-assisted OTEC cycle for power generation and fishery cold storage refrigeration, *Appl. Therm. Eng.* 90 (2015) 809–819, <https://doi.org/10.1016/j.applthermaleng.2015.07.072>.
- [18] A. Khosravi, S. Syri, M.E.H. Assad, M. Malekan, Thermodynamic and economic analysis of a hybrid ocean thermal energy conversion/photovoltaic system with hydrogen-based energy storage system, *Energy*. 172 (2019) 304–319, <https://doi.org/10.1016/j.energy.2019.01.100>.
- [19] A. Hasan, I. Dincer, An ocean thermal energy conversion based system for district cooling, ammonia and power production, *Int. J. Hydrogen Energy*. 45 (32) (2020) 15878–15887, <https://doi.org/10.1016/j.ijhydene.2020.03.173>.
- [20] W. Liu, X. Xu, F. Chen, Y. Liu, S. Li, L. Liu, Y. Chen, A review of research on the closed thermodynamic cycles of ocean thermal energy conversion, *Renew. Sustain. Energy Rev.* 119 (2020) 109581, <https://doi.org/10.1016/j.rser.2019.109581>.
- [21] C.C.K. Liu, Ocean thermal energy conversion and open ocean mariculture: The prospect of Mainland-Taiwan collaborative research and development, *Sustain. Environ. Res.* 28 (6) (2018) 267–273, <https://doi.org/10.1016/j.serj.2018.06.002>.
- [22] H. Ishaq, I. Dincer, A comparative evaluation of OTEC, solar and wind energy based systems for clean hydrogen production, *J. Clean. Prod.* 246 (2020) 118736, <https://doi.org/10.1016/j.jclepro.2019.118736>.
- [23] C. Bernardoni, M. Binotti, A. Giostri, Techno-economic analysis of closed OTEC cycles for power generation, *Renew. Energy*. 132 (2019) 1018–1033, <https://doi.org/10.1016/j.renene.2018.08.007>.
- [24] F. Yilmaz, Energy, exergy and economic analyses of a novel hybrid ocean thermal energy conversion system for clean power production, *Energy Convers. Manag.* 196 (2019) 557–566, <https://doi.org/10.1016/j.enconman.2019.06.028>.
- [25] Z. Wu, H. Feng, L. Chen, W. Tang, J. Shi, Y. Ge, Constructural thermodynamic optimization for ocean thermal energy conversion system with dual-pressure organic Rankine cycle, *Energy Convers. Manag.* 210 (2020) 112727, <https://doi.org/10.1016/j.enconman.2020.112727>.
- [26] S. Zhou, X. Liu, Y. Bian, S. Shen, Energy, exergy and exergoeconomic analysis of a combined cooling, desalination and power system, *Energy Convers. Manag.* 218 (2020) 113006, <https://doi.org/10.1016/j.enconman.2020.113006>.
- [27] S. Khanmohammadi, M.M. Baseri, P. Ahmadi, A.A.A. Al-Rashed, M. Afrand, Proposal of a novel integrated ocean thermal energy conversion system with flat plate solar collectors and thermoelectric generators: Energy, exergy and environmental analyses, *J. Clean. Prod.* 256 (2020) 120600, <https://doi.org/10.1016/j.jclepro.2020.120600>.
- [28] P. Ahmadi, I. Dincer, M.A. Rosen, Energy and exergy analyses of hydrogen production via solar-assisted ocean thermal energy conversion and PEM electrolysis, *Int. J. Hydrogen Energy*. 38 (4) (2013) 1795–1805, <https://doi.org/10.1016/j.ijhydene.2012.11.025>.
- [29] S.K. Wang, T.E. Hung, Renewable energy from the sea - Organic Rankine Cycle using ocean thermal energy conversion, in: *Proc. Int. Conf. Energy Sustain. Dev. Issues Strateg.* ESD 2010, IEEE Computer Society, 2010. <https://doi.org/10.1109/esd.2010.5598775>.
- [30] P.J.T. Straatman, W.G.J.H.M. van Sark, A new hybrid ocean thermal energy conversion-offshore solar pond (OTEC-OSP) design: A cost optimization approach, *Sol. Energy*. 82 (6) (2008) 520–527, <https://doi.org/10.1016/j.solener.2007.12.002>.
- [31] N.H. Mohd Idrus, M.N. Musa, W.J. Yahya, A.M. Ithnin, Geo-Ocean Thermal Energy Conversion (GeOTEC) power cycle/plant, *Renew. Energy*. 111 (2017) 372–380, <https://doi.org/10.1016/j.renene.2017.03.086>.
- [32] F. Yilmaz, M. Ozturk, R. Selbas, Thermodynamic performance assessment of ocean thermal energy conversion based hydrogen production and liquefaction process, *Int. J. Hydrogen Energy*. 43 (23) (2018) 10626–10636, <https://doi.org/10.1016/j.ijhydene.2018.02.021>.
- [33] S.M. Alirahmi, M. Rostami, A.H. Farajollahi, Multi-criteria design optimization and thermodynamic analysis of a novel multi-generation energy system for hydrogen, cooling, heating, power, and freshwater, *Int. J. Hydrogen Energy*. 45 (30) (2020) 15047–15062, <https://doi.org/10.1016/j.ijhydene.2020.03.235>.
- [34] E. Assareh, S.M. Alirahmi, P. Ahmadi, A Sustainable model for the integration of solar and geothermal energy boosted with thermoelectric generators (TEGs) for electricity, cooling and desalination purpose, *Geothermics*. 92 (2021) 102042, <https://doi.org/10.1016/j.geothermics.2021.102042>.
- [35] P. Ahmadi, I. Dincer, M.A. Rosen, Performance assessment of a novel solar and ocean thermal energy conversion based multigeneration system for coastal areas, *J. Sol. Energy Eng. Trans. ASME*. 137 (2015), <https://doi.org/10.1115/1.4028241>.
- [36] M. Nedaei, E. Assareh, M. Biglari, An extensive evaluation of wind resource using new methods and strategies for development and utilizing wind power in Mahshahr station in Iran, *Energy Convers. Manag.* 81 (2014) 475–503, <https://doi.org/10.1016/j.enconman.2014.02.025>.
- [37] S.B. Young, K. Brady, J. Fava, K. Saur, Eco-Efficiency and Materials: Foundation Paper by Five Winds International, n.d. www.icmm.com/page/1626/eco-efficiency-and-materials (accessed January 9, 2021).
- [38] S. Farahat, F. Sarhaddi, H. Ajam, Exergetic optimization of flat plate solar collectors, *Renew. Energy*. 34 (4) (2009) 1169–1174, <https://doi.org/10.1016/j.renene.2008.06.014>.
- [39] M. Zare, H. Ramin, S. Naemi, R. Hosseini, Exact optimum design of segmented thermoelectric generators, *Int. J. Chem. Eng.* 2016 (2016) 1–11, <https://doi.org/10.1155/2016/6914735>.
- [40] E. Houshfar, Thermodynamic analysis and multi-criteria optimization of a waste-to-energy plant integrated with thermoelectric generator, *Energy Convers. Manag.* 205 (2020) 112207, <https://doi.org/10.1016/j.enconman.2019.112207>.
- [41] A. Habibollahzade, E. Gholamian, P. Ahmadi, A. Behzadi, Multi-criteria optimization of an integrated energy system with thermoelectric generator, parabolic trough solar collector and electrolysis for hydrogen production, *Int. J. Hydrogen Energy*. 43 (31) (2018) 14140–14157, <https://doi.org/10.1016/j.ijhydene.2018.05.143>.
- [42] M. Soltani, M.H. Nabat, A.R. Razmi, M.B. Dusseault, J. Nathwani, A comparative study between ORC and Kalina based waste heat recovery cycles applied to a green compressed air energy storage (CAES) system, *Energy Convers. Manag.* 222 (2020) 113203, <https://doi.org/10.1016/j.enconman.2020.113203>.
- [43] A.R. Razmi, M. Janbaz, Exergoeconomic assessment with reliability consideration of a green cogeneration system based on compressed air energy storage (CAES), *Energy Convers. Manag.* 204 (2020) 112320, <https://doi.org/10.1016/j.enconman.2019.112320>.

- [44] E. Akrami, A. Chitsaz, H. Nami, S.M.S. Mahmoudi, Energetic and exergoeconomic assessment of a multi-generation energy system based on indirect use of geothermal energy, *Energy*. 124 (2017) 625–639, <https://doi.org/10.1016/j.energy.2017.02.006>.
- [45] H. Kianfard, S. Khalilarya, S. Jafarmadar, Exergy and exergoeconomic evaluation of hydrogen and distilled water production via combination of PEM electrolyzer, RO desalination unit and geothermal driven dual fluid ORC, *Energy Convers. Manag.* 177 (2018) 339–349, <https://doi.org/10.1016/j.enconman.2018.09.057>.
- [46] S.M. Alirahmi, S. Rahmani Dabbagh, P. Ahmadi, S. Wongwises, Multi-objective design optimization of a multi-generation energy system based on geothermal and solar energy, *Energy Convers. Manag.* 205 (2020) 112426, <https://doi.org/10.1016/j.enconman.2019.112426>.